# Investigation into Magnetic Control of Hard-Switching DC-DC Converters

J. Marcos Alonso
*Electrical Eng. Dept.*
*University of Oviedo*
Gijon, Spain
marcos@uniovi.es

Héctor Chinchero
*Electrical Eng. Dept.*
*University of Oviedo*
Gijon, Spain
UO248474@uniovi.es

Guirguis Z. Abdelmessih
*Electromechanical Eng. Dept.*
*University of Burgos*
Burgos, Spain
gzakiguirguis@ubu.es

Yueshi Guan
*Electrical Eng. Dept.*
*Harbin Institute of Technology*
Harbin, China
hitguanyueshi@163.com

Yijie Wang
*Electrical Eng. Dept.*
*Harbin Institute of Technology*
Harbin, China
wangyijie@hit.edu.cn

***Abstract* - In this paper an investigation into magnetic control (MC) of hard-switching (HS) DC-DC converters is carried out. The proposed control method is based on the modulation of the effective filter inductance of the converter when operating in discontinuous conduction mode (DCM). It is well known that the output characteristic of a HS DC-DC converter operating in DCM is dependent on the effective inductance of the output filter. This way, by using a variable inductance the output of the converter can be controlled. The proposed control method can be applied to any converter topology, namely buck, boost, buck-boost, flyback, forward, and so on. In this paper, the operation of the buck converter with MC is investigated in detail as a case study. This work proves that the proposed control method can be effectively used to control DC-DC converters on its own or by combination with other control parameters as duty cycle and/or frequency. An experimental prototype has been built to test the proposed control method and modeling process and to demonstrate its feasibility and possibilities.**

***Keywords* - magnetic devices, variable inductors, DC-DC converters, magnetic control, DCM operation.**

## I. INTRODUCTION

Switching DC-DC converters are used in a vast range of applications, including battery chargers, LED drivers, uninterruptible power supplies (UPS), housekeeping power supplies, point-of-load converters, etc. For low power applications, hard-switching (HS) DC-DC converters are the preferred option because of their simplicity, good efficiency, reliability and low component count. The most common and well-known topologies for low power applications are the buck, boost, buck-boost, flyback and forward converters. These converters can be controlled in a great variety of control methods, like voltage mode control and current-programmed control, which are primarily used. However, control methods proposed until now are based on directly or indirectly changing the switch duty cycle and/or switching frequency [1]. Magnetic regulators have been presented in previous literature as a means to improve the operation of power converters [2]-[23]. They have successfully been employed in controlling resonant inverters for electronic ballast [4]-[9], DC-DC converters [10]-[14], power converters for photovoltaic (PV) applications [15], power factor correction (PFC) converters [16][17], LED drivers [18]-[20], smart-grid applications [21], and battery charging [22][23].

This paper looks into the possibility of controlling HS DC-DC converters based on the modulation of the inductance used in the converter output filter. The goal of this work is the evaluation of the possibilities of this control method, which could be used in some niche applications on its own or by combination with duty cycle and/or frequency control. Some advantages of the proposed magnetic control can be identified as follows: i) constant frequency operation, ii) constant duty cycle operation, iii) implementation of multi-output converters with a reduced number of power switches, iv) additional control parameter for different control strategies, and v) simple dynamics, easy to stabilize in closed loop.

In order to introduce the proposed control method, which will be referred to as magnetic control (MC) of DC-DC converters, Fig. 1 illustrates a buck converter and its operating waveforms when working under continuous conduction mode (CCM) and discontinuous conduction mode (DCM).

Fig. 1a shows the current waveform through the inductor when the converter operates in CCM for two different values of the inductance $L_1$ and $L_2$ higher than $L_1$. As can be seen, when operating in CCM any change of the inductance will produce just a change on the inductor current ripple, while the average output current and voltage will keep the same. Therefore, it is not possible to use the inductance as control parameter for the output voltage and current when the converter operates in CCM. Nevertheless, in CCM the change in the inductance will produce a change on the dynamic response of the converter. The lower the inductance, the quicker the dynamic response of the converter. Thus, in CCM MC can be used to act upon the dynamic response of the converter to be adapted to load or input voltage changes. This idea has previously been investigated in [12].

On the other hand, Fig. 1b shows the inductor current waveforms when the converter is operating in DCM. In this case, the inductor has a direct effect on the average output current and voltage. As the value of the inductance increases, the average output current will decrease and so will do the average output voltage.

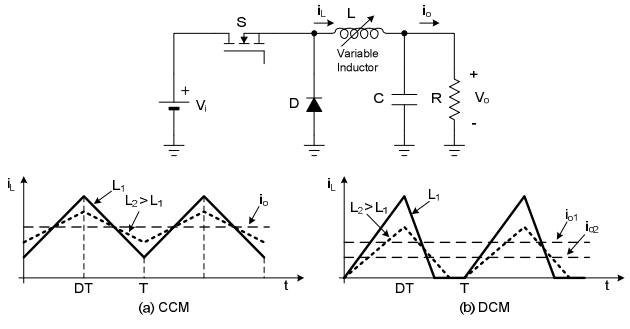


Fig. 1. Buck converter and operating waveforms under MC.

This work has been supported by the governments of Spain and Asturias under grants PID2019-105568RB-I00 and AYUD-2021-50938.

It is also possible to observe in Fig. 1b that as long as the inductance is increasing, the converter operation is approaching to CCM operation. Therefore, for a given switch duty cycle and switching frequency, there will be a maximum value of the inductance beyond which the buck converter will enter in CCM mode, and the output voltage and current will be fixed to that of the CCM characteristic, which as is well known will depend exclusively on the switch duty cycle in the ideal case. This paper is an updated version of the preprint document published in [29].

In the following, Section II presents the MC of DC-DC converters operating in DCM. Section III focuses on the study of the buck converter with MC, which has been selected as a case study to investigate the proposed control method. Section IV shows the implementation of the laboratory prototype and its experimental verification. Finally, Section V presents the conclusions that can be extracted from this work.

## II. Magnetic Control of DC-DC Converters under DCM Operation

### A. DC-DC DCM Converters with Magnetic Control

Fig. 1a and Fig. 2 show the schematic diagrams of the five basic DC-DC converters operating under MC: buck, boost, buck-boost, flyback and forward converters.

DC-DC converters have extensively been studied in CCM and DCM operation. From the studies presented in [1], it is possible to obtain the output characteristics of the different converters operating in DCM under MC. For this purpose, the normalized inductance $L_n$ of the converter is defined as follows:

$$L_n = \frac{L}{R/2f} \tag{1}$$

where $L$ is the inductance of the converter, and in the case of the flyback converter is the inductance seen from the primary side of the coupled inductors, $R$ represents the load resistance and $f$ is the converter switching frequency. Thus, Table I provides the output characteristic of the five converters and the condition of DCM operation from the point of view of the value of the controllable normalized inductance. In the equations of Table I, $D$ represents the switch duty cycle, and $n = N_s/N_p$ is the turn ratio of the flyback coupled inductors or the forward transformer, $N_s$ and $N_p$ being the turn numbers of secondary and primary windings respectively.

As can be seen from Table I, the voltage gain of the converters in DCM is a direct function of the inductance. This makes it possible to control the converter output voltage or current by means of inductance variation, i.e. by MC.

In order to provide a clearer insight on the static behavior of the different converters under MC, the output characteristics of Table I have been plotted in Fig. 3 and Fig. 4. Fig. 3 shows the output characteristic of the buck, boost and buck-boost converter. Fig. 4 illustrates the output characteristics of the flyback converter for a turn ratio $n = 0.5$, and of the forward converter for a turn ratio $n = 2$. As can be seen, in all characteristics there is a range corresponding to the DCM operation of the converter within which it is possible to control the output by changing the converter inductance. On the other hand, in the range corresponding to CCM operation, the voltage gain will remain constant; the change of the inductance has no effect on the average value of the output, affecting only the converter filter cut-off frequency and thus

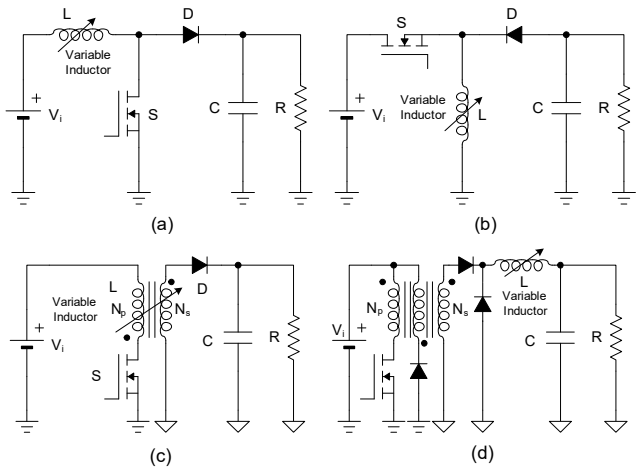


Fig. 2. DC-DC converters with MC: (a) boost, (b) buck-boost, (c) flyback and (d) forward.

the current and voltage ripples. For the flyback and forward converters, the effect of the turn ratio $n$ is to increase the DCM range of operation for the same voltage gain range, which is good because it is a manner of extending the range of output regulation of the converter.

TABLE I. Characteristics of DCM DC-DC Converters with MC.

| **Converter** | **Voltage Gain in DCM** $M = V_o/V_i$ | **Voltage Gain in CCM** $M = V_o/V_i$ | **DCM Condition** |
|---|---|---|---|
| Buck | $\dfrac{2}{1+\sqrt{1+\frac{4}{D^2}L_n}}$ | $D$ | $L_n \le 1-D$ |
| Boost | $\dfrac{1}{2}+\dfrac{1}{2}\sqrt{1+4D^2\dfrac{1}{L_n}}$ | $\dfrac{1}{1-D}$ | $L_n \le D(1-D)^2$ |
| Buck-boost | $D\sqrt{\dfrac{1}{L_n}}$ | $\dfrac{D}{1-D}$ | $L_n \le (1-D)^2$ |
| Flyback $n = N_s/N_p$ | $D\sqrt{\dfrac{1}{L_n}}$ | $\dfrac{nD}{1-D}$ | $L_n \le \dfrac{1}{n^2}(1-D)^2$ |
| Forward $n = N_s/N_p$ | $\dfrac{2n}{1+\sqrt{1+\frac{4}{D^2}L_n}}$ | $nD$ | $L_n \le (1-D)$ |
| $L_n = \dfrac{L}{R/2f}$ | | | |

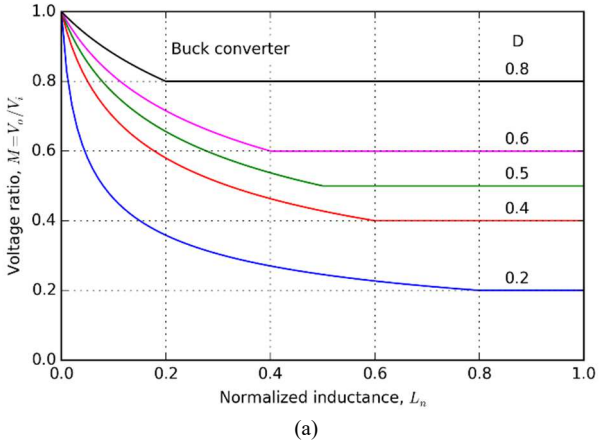


(a)

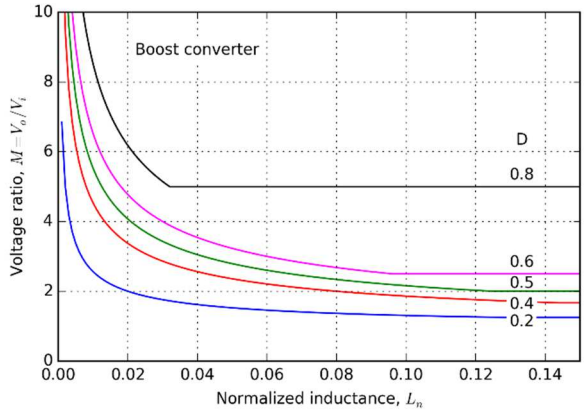


(b)

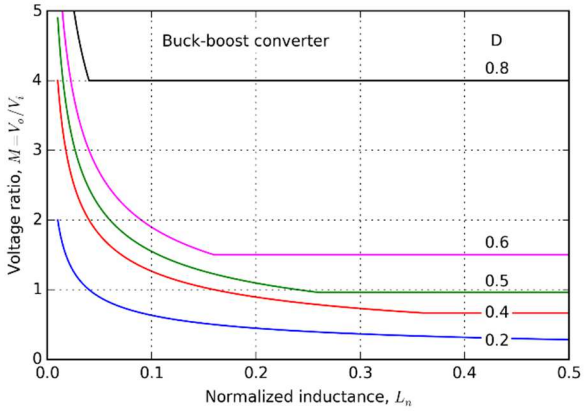


(c)

Fig. 3. Voltage ratio characteristics of the three basic non-isolated DC-DC converters with MC: (a) buck converter, (b) boost converter, and (c) buck-boost converter.

### *B. Implementation of Variable Inductors*

Variable inductors (VI) have been studied in previous literature [24]-[30]. These devices are capable of providing an inductance that can be controlled by a DC current injected into one or more auxiliary windings. The DC current generates a biasing magnetic flux that changes the DC operating point of the AC magnetic flux inside the core. This way, by moving the DC operating point along the B-H curve of the material close to the saturation knee, the permeability is changed, thus providing a variation of the effective inductance of the AC winding. Fig. 5 shows the scheme of two common VI; the double-E VI and the quad-U VI. These structures have previously been studied in [24]- [30], where it is possible to find more information on how to analyze, design and simulate these VI structures.

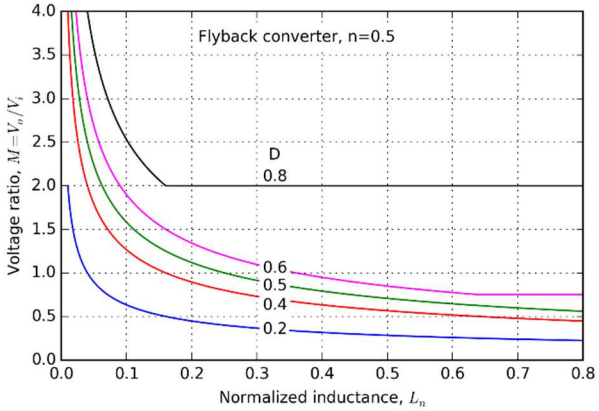


(a)

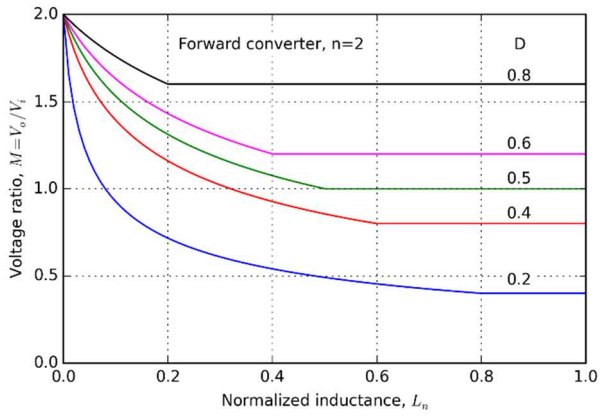


(b)

Fig. 4. Voltage ratio characteristics of the two basic isolated DC-DC converters with MC: (a) flyback converter, and (b) forward converter.

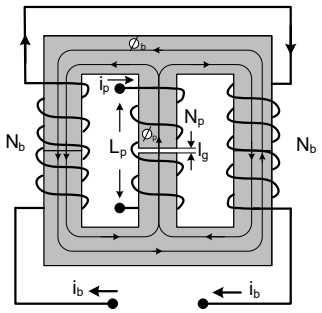


(a)

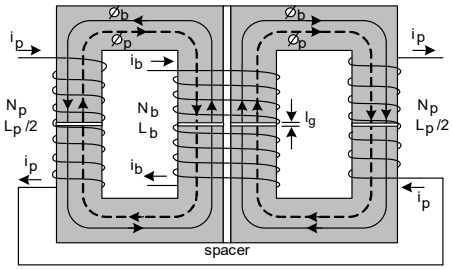


(b)

Fig. 5. Schematic of two VI structures: (a) double-E VI, (b) quad-U VI.

## III. Case Study: Buck Converter with Magnetic Control

In order to evaluate the possibilities of applying MC to DCM-operated DC-DC converters, a case study for the buck converter will be carried out in this section.

### *A. Static Analysis of the Buck Converter with Magnetic Control*

The static characteristics of the buck converter operating in DCM with MC can be obtained from the normalized characteristics shown in Table I. By substituting the normalized inductance given by (1), the following expression can be obtained for the converter voltage gain $M$:

$$M=\frac{V_o}{V_i}=\frac{2}{1+\sqrt{1+\frac{8fL}{D^2R}}} \quad if\ L\le(1-D)\frac{R}{2f}$$
$$M=\frac{V_o}{V_i}=D \quad if\ L\ge(1-D)\frac{R}{2f} \tag{2}$$

As an example, Fig. 6 shows the voltage gain characteristics of the buck converter for a particular case with duty cycle $D=$

0.4, switching frequency $f = 100\ kHz$ and inductance up to $25\ \mu H$, which have been obtained by plotting (2). As can be seen, for a given load resistance DCM operation is achieved for the lower values of the converter inductance. When the critical inductance value is reached, the converter enters in CCM operation and the voltage gain becomes constant and equal to the converter duty cycle, $D$. Voltage regulation can only be achieved in DCM operation.

### *B. Proposed Control Scheme*

The proposed control scheme of the buck converter operating in DCM mode with MC is illustrated in Fig. 7. As can be seen, the circuit is quite simple. The output voltage is measured by a voltage divider and fed into a lag-lead compensator, which drives the bipolar transistor Q in order to generate the required bias current $i_b$ for the variable inductor. For a proper design of the compensator parameters, the dynamic model of the buck converter with MC must be obtained. This analysis will be presented in the next section.

### *C. Dynamic Model of the Buck Converter with Magnetic Control*

In this section, the basic dynamic analysis of the buck converter with MC will be presented. With reference to the control scheme previously presented in Fig. 7, the objective of the analysis is to obtain the transfer function $G_{ol}(s)$ that relates the inductance perturbation $l(s)$ with the output voltage perturbation $v_o(s)$, this is:

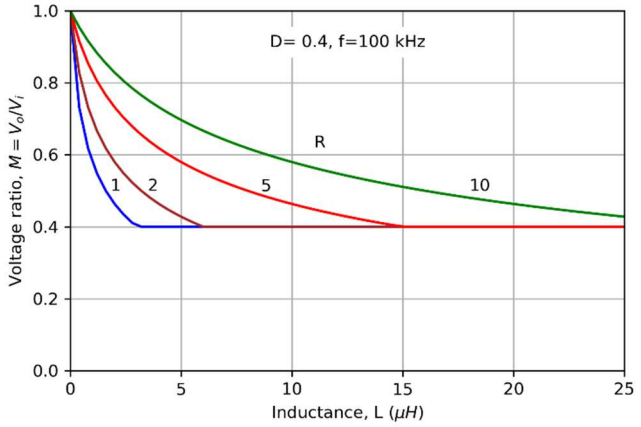


Fig. 6. Voltage gain of a buck converter as a function of the converter inductance for different load resistances.

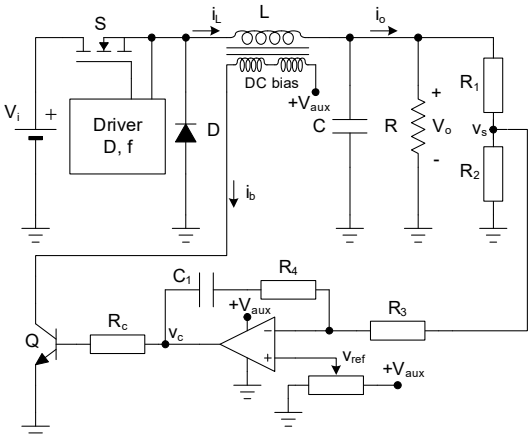


Fig. 7. Proposed control scheme of the DCM operated buck converter with MC.

$$G_{ol}(s) = \frac{v_o(s)}{l(s)} \tag{3}$$

Fig. 8 shows the equivalent circuits of the buck converter operating in DCM in the averaged time domain, Fig. 8a, and in the Laplace variable domain, Fig. 8b. The effect of the series resistance of the filter capacitor have been neglected for simplicity assuming that a film capacitor with very low series resistance will be used; nevertheless, it could easily be taken into account. The inductor average current of the buck converter in DCM mode can be calculated as follows:

$$\langle i_L \rangle = \frac{D^2 V_i}{2f}\left(\frac{V_i}{V_o} - 1\right)\frac{1}{L} \tag{4}$$

By taking partial derivative with respect to $L$ and using the Laplace transform, the following relationship is obtained between the inductor current and inductor perturbations:

$$i_L(s) = k_{il}\, l(s) \tag{5}$$

where

$$k_{il} = -\frac{D^2 V_i}{2f}\left(\frac{V_i}{V_o} - 1\right)\frac{1}{L^2} \tag{6}$$

Now, solving the circuit shown in Fig. 8b for the output voltage, the buck converter dynamics between the output voltage and inductor can be obtained, as follows:

$$G_{ol}(s) = \frac{v_o(s)}{l(s)} = k_{ol}\frac{1}{1 + s/\omega_p} \tag{7}$$

where

$$k_{ol} = k_{il} R \tag{8}$$

$$\omega_p = \frac{1}{RC} \tag{9}$$

As stated in [20], it is a good approximation to neglect the dynamics between VI bias flux perturbations $B_b(s)$ and VI inductance perturbations $l(s)$ because these dynamics will be of a higher order of magnitude in comparison with the other dynamics of the VI. Therefore, the following expression can be written:

$$l(s) \approx k_{lb}\, B_b(s) \tag{10}$$

where $k_{lb}$ is the proportionality constant that relates inductance and bias flux perturbations. The procedure to derive this constant can be found in [30].

Also, the bias flux and bias current $i_b(s)$ perturbations can be related by the following expression:

$$B_b(s) = \frac{L_{b\_eff}}{2N_b A_b}\, i_b(s) \tag{11}$$

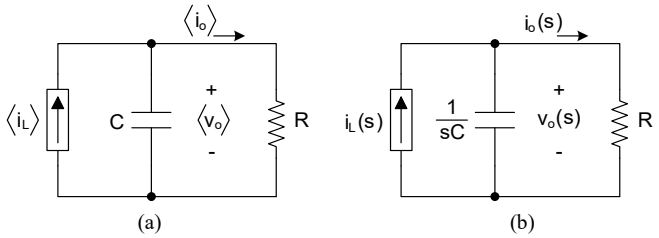


Fig. 8. Equivalent circuits of the buck converter with MC: (a) averaged time domain, and (b) Laplace variable domain.

where $L_{b\_eff}$, $N_b$ and $A_b$ are the effective inductance [20], turn number, and effective section of the auxiliary bias winding, respectively.

Note that in (11) the factor 2 before $N_b$ is necessary because the total bias inductance is given by two bias windings in series, each one with a number of turns equal to $N_b$.

Using (11) in (10), a direct relationship between inductance and bias current perturbations can be obtained:

$$l(s) \approx k_{li}\, i_b(s) \tag{12}$$

where:

$$k_{li} = \frac{k_{lb}\, L_{b\_eff}}{2N_b A_b} \tag{13}$$

It must be noted that the constant $k_{li}$ corresponds to the slope of the characteristic of inductance versus bias current of the VI at the given operating point, which can be obtained theoretically following the process shown in [24][27].

With regard to the dynamics between the compensator output signal $v_c$ and the bias winding current $i_b$, it has already been studied in [20]. It can be expressed as follows:

$$G_{bc}(s) = \frac{i_b(s)}{v_c(s)} = \frac{k_{bc}}{1 + s/\omega_c} \tag{14}$$

where

$$k_{bc} = \frac{h_{fe}}{R_c + h_{ie}} \cdot \frac{1}{1 + h_{oe}R_b} \tag{15}$$

$$\omega_c = \frac{h_{oe}^{-1} + R_b}{L_{b\_eff}} \tag{16}$$

where $h_{ie}$, $h_{fe}$ and $h_{oe}$ are the $h$ parameters of the small-signal model of the bipolar transistor used in the bias winding, namely input impedance, forward current gain, and output admittance respectively. These parameters can be obtained from the transistor datasheet if available. Other option is to extract the parameters from its SPICE model by computer simulation [30].

Fig. 9 shows the complete block diagram of the dynamic model of the buck converter operating with MC. The following transfer function can be defined to represent the dynamic behavior from the control voltage $v_c$ to the output voltage $v_o$:

$$G_o(s) = \frac{v_o(s)}{v_c(s)} = k_{li} G_{bc}(s) G_{ol}(s) \tag{17}$$

which corresponds to a transfer function with two poles given by $\omega_p$ and $\omega_c$ in (9) and (16) respectively.

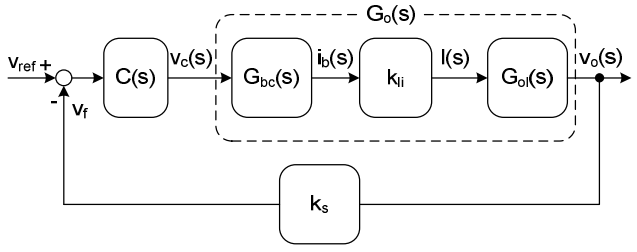


Fig. 9. Block diagram of the dynamic model of the buck converter with MC.

The gain of the feedback network is determined by $R_1$ and $R_2$ in Fig. 7, as follows:

$$k_s = \frac{R_2}{R_1 + R_2} \tag{18}$$

## IV. Experimental Results

As an example of implementation, a buck converter operating at a switching frequency of 100 kHz and with a duty cycle of 0.4 (on time, $t_{on} = 4\,\mu s$) will be presented and studied in this section. According to the characteristics of Fig. 6, a VI ranging from 5 $\mu H$ to 20 $\mu H$ has been implemented with the parameters shown in Table II. Fig. 10 shows the characteristic of inductance versus bias current of the implemented VI.

The buck converter is supplied with 10 V input voltage and nominal load resistance of 5 Ω. The output filter capacitance is 33 µF, implemented with a film capacitor so that its series resistance can be neglected. Table III summarizes the parameters of the implemented prototype. The $h$ parameters of the BD139 bipolar transistor used in the bias circuit have been obtained from the SPICE model of the transistor by simulation under LTspice, as shown in [30].

Based on the analysis presented in Section II.C, the dynamic response of the converter with MC has been obtained. Fig. 11 shows this response, corresponding to the bode diagram of amplitude and phase of output voltage $v_o(s)$ over control voltage $v_c(s)$, which has been designated as $G_o(s)$ in Section II.C. From this theoretical analysis, the pole corresponding to the buck output filter as given by (9) is obtained at 964 Hz, while the pole due to the VI response, given by (16), appears at 35.2 kHz. The DC gain of the system is 8.96 dB.

TABLE II. PARAMETERS OF THE IMPLEMENTED VI.

| **Parameter** | **Type/Value** |
|---|---|
| Structure | Double E |
| Core | EFD25/13/9, N87 |
| Main winding | N=12, 66x0.08 mm (litz) |
| Central arm cross-sectional area | $A_c$= 59.3 mm$^2$ |
| Central arm length | $l_c$= 24.4 mm |
| Middle arm gap | $l_{gc}$= 0.6 mm |
| Lateral arms gap | $l_{ge}$= 0 mm |
| Bias windings | 2 x $N_b$= 65, 1x0.2 mm |
| Outer arms cross-sectional area | $A_e$=28.7 mm$^2$ |
| Outer arms length | $l_e$= 43.6 mm |
| Main inductance range | 5 µH – 20 µH |
| Bias winding effective series inductance and resistance | 1.2 mH / 6.2 Ω @ 100 Hz |

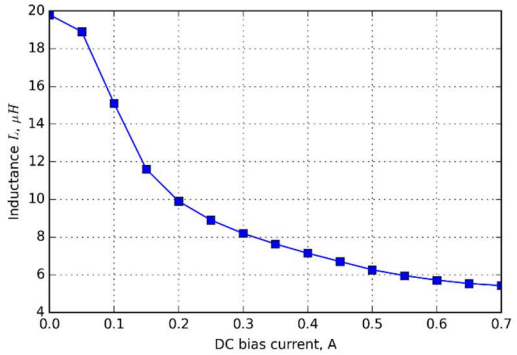


Fig. 10. Measured characteristic of inductance versus bias current of the implemented VI.

TABLE III. PARAMETERS OF THE IMPLEMENTED BUCK CONVERTER WITH MC.

| **Parameter** | **Type/Value** |
|---|---|
| Input voltage | 10 V |
| Output voltage | 5 V |
| Duty cycle | 0.4 |
| Switching frequency | 100 kHz |
| Inductor | 5 µH – 20 µH |
| Capacitor | 33 µF |
| Nominal load resistance | 5 Ω |
| Power switch | IRFZ48 |
| Diode | 11DQ10 |
| Bias winding transistor model parameters | BD139 / $h_{fe} = 43.8, h_{ie} = 28.2\ \Omega, h_{oe} = 0.0079\ \Omega^{-1}$ |
| Bias winding transistor base resistance | $R_c$= 100 Ω |
| Voltage sensing resistances | $R_1$, $R_2$= 10 kΩ |

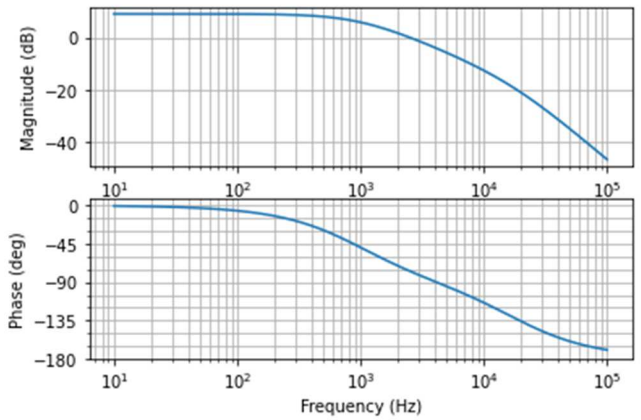


Fig. 11. Theoretical bode diagram of the converter in open loop, corresponding to the transfer function $G_o(s)$ in the block diagram of Fig. 9.

The characteristic of output voltage $v_o$ versus control voltage $v_c$ operating with duty cycle of 0.4 and load resistance of 5 Ω has been measured at the laboratory. Fig. 12 shows the resulting curve. The squares show the experimental measurement, while the dashed line shows an approximation obtained by exponential regression. As can be seen, the output voltage can be controlled within a reasonably wide range by means of the control voltage $v_c$, which changes the effective value of the converter inductance.

As previously explained, the slope of the output control curve shown in Fig. 12 can be used to obtain the total DC gain of the converter control function $G_o(s)$. For example, around the nominal operating point of 5 V at the output, the slope can be approximated to 3.61 (11.1 dB).

Fig. 13 shows the buck converter LC-filter input voltage and the VI current in two different situations of output voltage and current. Fig. 13a corresponds to an output voltage and current of 5 V and 1 A respectively. As can be seen, the converter is operating at the critical conduction mode (DCM-CCM boundary). Fig. 13b shows the waveforms for an output voltage and current of 5.5 V and 1.1 A. As can be seen, in this case the converter is clearly operating in DCM mode. This is because to increase the output voltage the VI inductance must be decreased, which according to the characteristics in Fig. 3a and Fig. 6, forces the operation to go further into DCM mode.

The second test performed on the prototype was to measure the system dynamics by acquiring the bode diagram of the system transfer function $G_o(s)$. An Omicron Bode 100 has been used for this operation. Fig. 14 shows the obtained results. As can be seen, the response matches with quite good accuracy the theoretical response shown previously in Fig. 11, which validates the developed dynamic model.

In order to test the system regulation in closed loop, a lag-lead compensator as the one illustrated in Fig. 7 has been designed. Table IV shows the parameters of the implemented compensator.

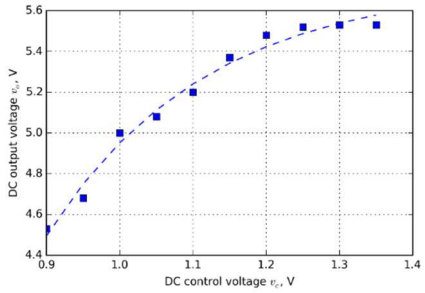


Fig. 12. Characteristic of output voltage versus control voltage of the buck converter with MC. Squares: experimental measurement; dashed line: approximation by exponential curve fitting.

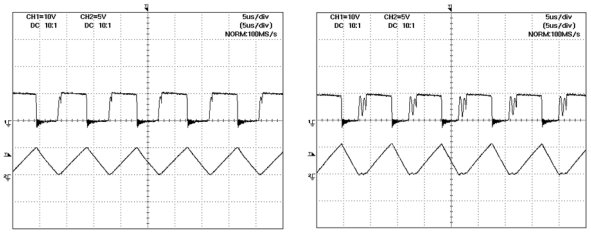

(a) (b)

Fig. 13. Buck filter input voltage and VI current in two different situations: (a) $V_o = 5V, I_o = 1\ A$; (b) $V_o = 5.5\ V, I_o = 1.1\ A$. Scales: 10 V/div, 1 A/div, 5 µs/div.

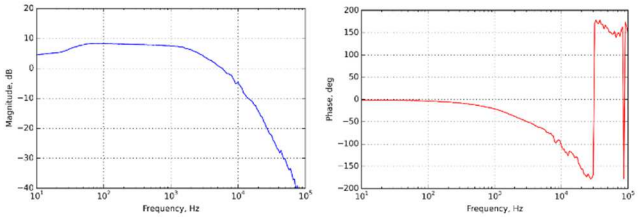


Fig. 14. Experimental response of the control transfer function $G_o(s)$ corresponding to the implemented buck converter with MC.

TABLE IV. PARAMETERS OF THE IMPLEMENTED LAG-LEAD COMPENSATOR.

| Parameter | Type/Value |
|---|---|
| High frequency gain | 0 dB |
| Zero's frequency | 1 kHz |
| Operational amplifier | LM358 |
| Resistances $R_3, R_4$ | 16 $k\Omega$ |
| Capacitance $C_1$ | 10 nF |

Fig. 15 shows the experimental loop gain magnitude and phase of the buck converter with MC when using the compensator shown in Table IV. The measurement was taken using the voltage injection method, with an injection transformer B-WIT 100 from Omicron. As can be seen, the loop gain response is in accordance with the theoretical analysis. The system is well stabilized with a phase margin of around 110 degrees and a gain margin of around 40 dB.

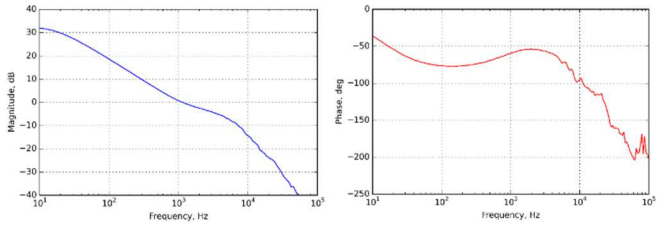


Fig. 15. Experimental loop gain and phase of the buck converter operating with a lag-lead compensator and MC.

Fig. 16 shows experimental responses of the buck converter operating in closed loop with the proposed MC. Fig. 16a shows the output voltage response for a load step between 5 Ω and 10 Ω. The output voltage response is in accordance with the expected one since it corresponds to a first order response with a settling time around 500 µs. Fig. 16b shows the output voltage response for an input voltage change between 8 V and 11 V. A first order response with a settling time around 500 µs is also obtained, which is in accordance with the system closed-loop design.

Table V and VI show the experimental measurements corresponding to the load regulation (Table V) and line regulation (Table VI). The values of the control signal $v_c$ generated by the compensator and those of the dc current through the bias winding $i_b$ are also provided to show the operation of the closed-loop regulation. As can be seen in both tables, even though the control range is not very wide for this particular design, the output voltage is well regulated for both load and line changes, thus proving the feasibility of the proposed control methodology.

## V. CONCLUSIONS

The magnetic control of DC-DC converters operating in DCM has been investigated in this paper. The important control characteristics of the most relevant converters operating with MC have been presented, demonstrating that it is possible to use the converter filter inductance as control parameter to regulate output voltage or current.

The buck converter has been selected as case study to evaluate the possibilities of MC of DC-DC converters. The dynamic model of the MC DCM buck converter proves to be similar to that resulting from other control methods, as voltage, current-programmed or frequency-sweep mode control. Since the converter operates in DCM, it keeps its first order behavior, exhibiting a main pole given by the filter capacitance and load resistance. The MC introduces a second pole defined by the effective inductance of the VI bias winding and by the addition of the output resistance of the current source used to drive the bias winding and the series resistance of the bias winding itself.

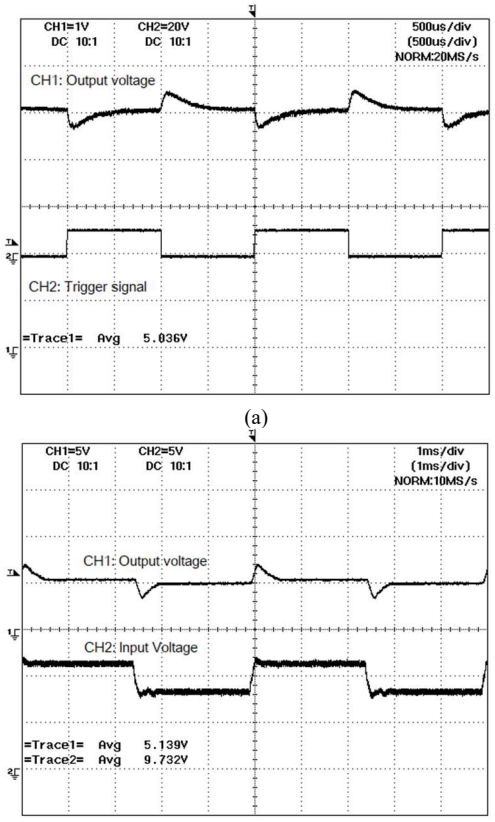


Fig. 16. Experimental closed-loop response of the magnetically controlled buck converter with a lag-lead compensator: (a) Output voltage transient for a load step change between 5 Ω and 10 Ω, (b) Output voltage transient for an input voltage step between 8 V and 11 V. CH1, CH2 and time scales are as labelled in the figures.

TABLE V. EXPERIMENTAL RESULTS: LOAD REGULATION FOR 10 V INPUT VOLTAGE

| Output Current (A), $I_o$ | Output Voltage (V), $V_o$ | Control Voltage (V), $v_c$ | VI Bias Current (A), $i_b$ |
|---|---|---|---|
| 1.15 | 5.01 | 1.10 | 0.38 |
| 0.98 | 5.01 | 0.93 | 0.24 |
| 0.83 | 5.02 | 0.87 | 0.17 |
| 0.71 | 5.02 | 0.82 | 0.13 |
| 0.62 | 5.02 | 0.79 | 0.09 |
| 0.52 | 5.03 | 0.74 | 0.06 |
| 0.48 | 5.03 | 0.73 | 0.04 |

TABLE VI. EXPERIMENTAL RESULTS: LINE REGULATION FOR 5 Ω LOAD RESISTANCE.

| Input Voltage (V), $V_i$ | Output Voltage (V), $V_o$ | Output Current (A), $I_o$ | Control Voltage (V), $v_c$ | VI Bias Current (A), $i_b$ |
|---|---|---|---|---|
| 8.5 | 4.83 | 1.00 | 2.86 | 0.85 |
| 9.0 | 4.99 | 1.03 | 1.27 | 0.47 |
| 9.5 | 5.00 | 1.04 | 1.04 | 0.35 |
| 10.0 | 5.00 | 1.04 | 0.93 | 0.25 |
| 10.5 | 5.01 | 1.04 | 0.90 | 0.21 |
| 11.0 | 5.02 | 1.04 | 0.80 | 0.09 |

The obtained experimental results have proven the theoretical model of the MC buck converter. It has also been demonstrated how the converter can be closed-loop controlled with a simple lag-lead controller that can be designed based on conventional methods. The experimental measurement of the converter loop gain, and the load and input-voltage step responses are in full agreement with the closed-loop design of the converter.

As an additional conclusion, MC DC-DC converters can be used in other applications, such as in LED drivers, electric vehicle charging, DC motor control, PV converters, smart-grid converters, PFC converters, wireless power transfer, etc.

## REFERENCES


[1] M. K. Kazimierczuk; Pulse Width Modulated DC-DC Power Converters. Wiley, 2008.

[2] A. S. Kislovski, "Quasi-linear controllable inductor," Proc. of the IEEE, vol. 75, No. 2, Feb. 1987, pp. 267-269.

[3] M. S. Perdigao, M. Menke, A. R. Seidel, R. A. Pinto, J. M. Alonso, "A review on variable inductors and variable transformers: Applications to lighting drivers," IEEE Trans. on Ind. App., Jan. 2016.

[4] M. Gulko, D. Medini and S. Ben-Yaakov, "Inductor-controlled current-sourcing resonant inverter and its application as a high pressure discharge lamp driver," Proc. of 1994 IEEE App. Power Electr. Conf. and Exp. - APEC'94, Orlando, FL, USA, 1994, pp. 434-440 vol.1.

[5] J. M. Alonso, M. A. Dalla Costa, M. Rico-Secades, J. Cardesín, J. Garcia, "Investigation of a New Control Strategy for Electronic Ballasts Based on Variable Inductor", IEEE Trans. on Ind. Electr., Vol. 55, Nº 1, pp. 3-10, Jan. 2008.

[6] M. F. Menke, M. F. da Silva, A. R. Seidel, M. S. Perdigão and J. M. Alonso, "High power factor dimmable self-oscillating electronic ballast with variable inductor control," IEEE App. Power Electr. Conf. and Expo. (APEC), 2015, Charlotte, NC, 2015, pp. 3314-3321.

[7] M. S. Perdigao, J. M. Alonso, M. A. Dalla Costa, E. S. Saraiva, "Comparative Analysis and Experiments of Resonant Tanks for Magnetically Controlled Electronic Ballasts," Ind. Electr., IEEE Trans. on, vol.55, no.9, pp. 3201-3211, Sept. 2008.

[8] M. S. Perdigao, J. M. Alonso, M. A. Dalla Costa, E. S. Saraiva, "Using Magnetic Regulators for the Optimization of Universal Ballasts," IEEE Trans. on Power Electr., vol.23, no.6, pp. 3126-3134, Nov. 2008.

[9] U. Boeke, "Scalable fluorescent lamp driver using magnetic amplifiers," European Power Electr. Conf. and Expo. (EPE), pp. 1-10, 2005.

[10] J. M. Alonso, M. S. Perdigão, D. G. Vaquero, A. J. Calleja, E. S. Saraiva, "Analysis, Design, and Experimentation on Constant-Frequency DC-DC Resonant Converters With Magnetic Control," IEEE Trans. on Power Electr., vol. 27, no. 3, pp. 1369-1382, March 2012.

[11] Q. M. Luo, H. Yan, S. Chen and L. W. Zhou, "Interleaved high step-up zero-voltage-switching boost converter with variable inductor control," in IET Power Electr., vol. 7, no. 12, pp. 3083-3089, 12 2014.

[12] S. M. Ahsanuzzaman ; Timothy McRae ; Mor M. Peretz ; Aleksandar Prodić; "Low-volume buck converter with adaptive inductor core biasing," Proc. of IEEE Applied Power Electronics Conference and Exposition (APEC), pp. 335 – 339, 2012.

[13] Y. Wei, Q. Luo, J. M. Alonso and A. Mantooth, "A Magnetically Controlled Single-Stage AC–DC Converter," in IEEE Transactions on Power Electronics, vol. 35, no. 9, pp. 8872-8877, Sept. 2020.

[14] M. W. Beraki, J. P. F. Trovão, M. S. Perdigão and M. R. Dubois, "Variable Inductor Based Bidirectional DC–DC Converter for Electric Vehicles," in IEEE Trans. on Vehicular Tech., vol. 66, no. 10, pp. 8764-8772, Oct. 2017.

[15] L. Zhang, W. G. Hurley and W. Wölfle, "A new approach to achieve maximum power point tracking for PV system with a variable inductor," The 2nd International Symposium on Power Electronics for Distributed Generation Systems, Hefei, 2010, pp. 948-952.

[16] C.-Y. Lim, J. H. Kim, Y. Jeong, D.-K Kim, H.-S. Youn, G.-W. Moon, "A high efficiency critical mode boost PFC using a variable inductor," 2016 IEEE 8th Int. Power Electr. and Motion Control Conf. (IPEMC-ECCE Asia), Hefei, 2016, pp. 2792-2797.

[17] Y. Wei, Q. Luo, J. M. Alonso and A. Mantooth, "A Magnetically Controlled Single-Stage AC–DC Converter," in IEEE Transactions on Power Electronics, vol. 35, no. 9, pp. 8872-8877, Sept. 2020.

[18] R. A. Pinto, J. M. Alonso, M. S. Perdigão, M. F. da Silva and R. N. do Prado, "A New Technique to Equalize Branch Currents in Multiarray LED Lamps Based on Variable Inductors," in IEEE Trans. on Industry Applications, vol. 52, no. 1, pp. 521-530, Jan.-Feb. 2016.

[19] Y. Hu, L. Huber and M. M. Jovanović, "Single-Stage, Universal-Input AC/DC LED Driver with Current-Controlled Variable PFC Boost Inductor," in IEEE Transactions on Power Electronics, vol. 27, no. 3, pp. 1579-1588, March 2012.

[20] J. M. Alonso, M. Perdigao, M. A. Dalla Costa, G. Martínez and R. Osorio, "Analysis and Experiments on a Single-Inductor Half-Bridge LED Driver with Magnetic Control," IEEE Trans. on Power Electronics, vol. 32, no. 12, 9179-9190.

[21] S. Saeed and J. Garcia, "Extended Operational Range of Dual-Active-Bridge Converters by using Variable Magnetic Devices," 2019 IEEE Applied Power Electronics Conference and Exposition (APEC), Anaheim, CA, USA, 2019, pp. 1629-1634.

[22] Y. Wei, Q. Luo, X. Du, N. Altin, A. Nasiri and J. M. Alonso, "A Dual Half-Bridge LLC Resonant Converter With Magnetic Control for Battery Charger Application," in IEEE Transactions on Power Electronics, vol. 35, no. 2, pp. 2196-2207, Feb. 2020.

[23] Y. Wei, Q. Luo, S. Chen, Q. He and L. Zhou, "A High Efficiency Single Stage Bi-directional Battery Charger with Magnetic Control," 2018 IEEE Int. Power Electronics and Application Conf. and Exp. (PEAC), Shenzhen, 2018, pp. 1-6.

[24] J. M. Alonso, M. Perdigão, M. A. Dalla Costa, S. Zhang and Y. Wang, "Variable inductor modeling revisited: The analytical approach," 2017 IEEE Energy Conv. Congr. and Exp. (ECCE), Cincinnati, OH, 2017, pp. 895-902.

[25] J. M. Alonso, G. Martínez, M. Perdigão, M. R. Cosetin and R. N. do Prado, "A Systematic Approach to Modeling Complex Magnetic Devices Using SPICE: Application to Variable Inductors," in IEEE Trans. on Power Electr., vol. 31, no. 11, pp. 7735-7746, Nov. 2016.

[26] J. M. Alonso, M. Perdigao, G. Z. Abdelmessih, M. A. Dalla Costa, Y. Wang, "SPICE Modeling of Variable Inductors and its Application to Single Inductor LED Driver Design," in IEEE Trans. on Ind. Electr., vol. 64, No. 7, 5894-5903, Jul. 2017.

[27] J. M. Alonso, M. Perdigão, M. A. Dalla Costa, S. Zhang, Y. Wang; "Analysis and experimentation of the quad-U variable inductor for power electronics applications," IET Power Electronics, 11 (14), 2330-2337, 2019.

[28] H. Chinchero and J. M. Alonso, "Using Magnetic Control of DC-DC Converters in LED Driver Applications," in IEEE Latin America Transactions, vol. 19, no. 02, pp. 297-305, February 2021.

[29] J. M. Alonso, H. Chinchero, G. Z. Abdelmessih, Y. Guan, Y. Wang; "Investigation into Magnetic Control of Hard-Switching DC-DC Converters," TechRxiv. Preprint. 2020.

[30] J. M. Alonso; Inductors: Variable and Controllable. Amazon KDP, ISBN 979-85-00248-16-9, 2021.